# Engineering Ternary Copper-Cobalt Sulfide Nanosheets as High-performance Electrocatalysts toward Oxygen eVolution Reaction

**Heng Luo [1,†], Hang Lei [1,2,†], Yufei Yuan [3], Yongyin Liang [1], Yi Qiu [1,2], Zonglong Zhu [3] and Zilong Wang [1,*]**

[1]  Siyuan Laboratory, Guangdong Provincial Engineering Technology Research Center of Vacuum Coating Technologies and New Energy Materials, Department of Physics, Jinan University, Guangzhou 510632, China; hengluo98@163.com (H.L.); jnleihang@gmail.com (H.L.); eVelyn2246@163.com (Y.L.); yiqiu_16@163.com (Y.Q.)
[2]  Department of Chemistry, Jinan University, Guangzhou, Guangdong 510632, China
[3]  Department of Chemistry, City University of Hong Kong, Kowloon, Hong Kong; yufeiyuan2-c@my.cityu.edu.hk (Y.Y.); zonglzhu@cityu.edu.hk (Z.Z.)
*  Correspondence: zilong@email.jnu.edu.cn; Tel.: +86-85224386-307
†  These authors contributed equally to this work.

**Abstract:** The rational design and development of the low-cost and effective electrocatalysts toward oxygen eVolution reaction (OER) are essential in the storage and conversion of clean and renewable energy sources. Herein, a ternary copper-cobalt sulfide nanosheets electrocatalysts (denoted as CuCoS/CC) for electrochemical water oxidation has been synthesized on carbon cloth (CC) via the sulfuration of CuCo-based precursors. The obtained CuCoS/CC reveals excellent electrocatalytic performance toward OER in 1.0 M KOH. It exhibits a particularly low overpotential of 276 mV at current density of 10 mA cm$^{-2}$, and a small Tafel slope (58 mV decade$^{-1}$), which is superior to the current commercialized noble-metal electrocatalysts, such as IrO$_2$. Benefiting from the synergistic effect of Cu and Co atoms and sulfidation, electrons transport and ions diffusion are significantly enhanced with the increase of active sites, thus the kinetic process of OER reaction is boosted. Our studies will serve as guidelines in the innovative design of non-noble metal electrocatalysts and their application in electrochemical water splitting

**Keywords:** oxygen eVolution reaction; water oxidation; ternary copper-cobalt sulfide; nanosheets

## 1. Introduction

Faced with the environmental problems and climate changes that are caused by the consumption of increasingly exhausted traditional fossil fuels, it is indispensable to build a sustainable energy system and develop clean and pollution-free energy instead of conventional energy sources in the future [1–3]. Hydrogen is widely regarded as a clean, renewable, and environmentally friendly energy carrier, which attracts wide attention in various fields [4–6]. By far, among the many hydrogen production methods (methane oxidation or reforming, etc.), electrochemical water splitting is considered to be the most promising one at present, because it provides an apinoid strategy for renewable energy conversion and storage [7–10]. However, the semi-reaction in the process of water splitting, oxygen eVolution reaction (OER), is related to the continuous process of four proton-coupled electron transfer, which requires a higher overpotential at the anode and it therefore undergoes a sluggish reaction dynamics process [11–13]. As a consequence, it is particularly valuable for researchers to develop efficient and stable oxygen-evolving catalysts at present [14,15]. Particularly, some noble metal catalysts, including

$IrO_2$ and $RuO_2$, are deemed to the most efficient and robust electrocatalysts for water oxidation [16,17]. Nevertheless, the fancy price and low reserves of noble metals limit the extensive application of catalysts in industry and business [18]. Thus, rational design and the manufacture of highly active, inexpensive, and durable non-noble metal electrocatalysts are desirable and challenging [19].

Recently, transition metal sulfides, as one of the non-noble metal electrocatalysts, have attracted numerous research interests due to their similar catalytic activity to noble metals, unique physicochemical properties, and low cost [20,21]. Especially, because of cobalt sulfide's ($CoS_2$) intrinsic metal peculiarity, excellent electrical conductivity, and chemical stability, it is widely used in electrolytic oxygen eVolution reaction [22,23]. On the other hand, for dopants, the valence and phase diversity of copper-cobalt, as well as the relatively rich redox chemistry, are considered as ideal catalytic materials for water oxidation catalysts [24]. What is more, multicomponent copper-based sulfides are widely used in many fields due to their superior carrier concentration and charge transfer characteristics [25,26]. The synergistic effect of bimetallic construction between copper and other types of atoms is beneficial in the optimization of electronic structure, increasing the number of active sites, and improving conductivity, and it will greatly promote the activity of electrocatalysis [27–30]. Nowadays, Copper-cobalt complex sulfides have been extensively studied in the field of energy storage, such as supercapacitors [31–33]. However, the application of electrocatalytic oxygen eVolution reaction is still less reported, so there are still some challenges and arduous research tasks.
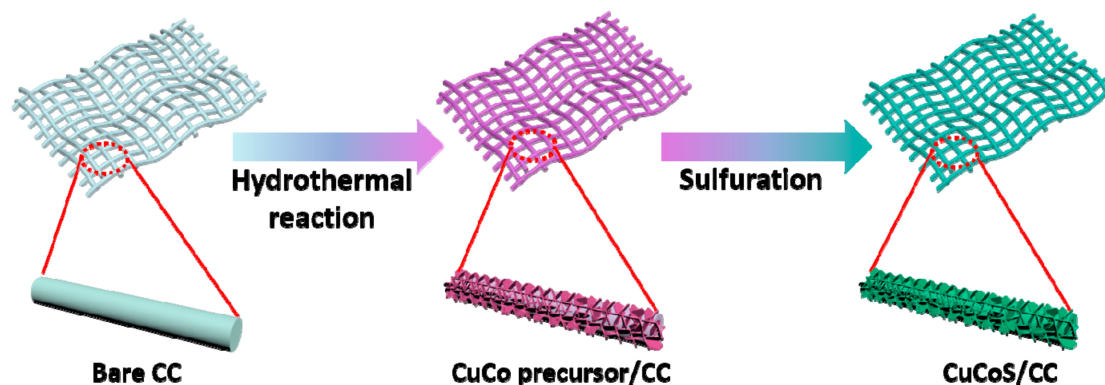
As is known to all, copper and cobalt have similar chemical properties, such as atomic radius and ionization energy, so this is favorable in the formation of bimetallic compounds. Herein, based on the viewpoints that are mentioned above, we designed and developed novel ternary copper-cobalt sulfide nanosheets that were loaded in carbon cloth (CuCoS/CC) as catalysts for OER in alkaline media by one-step hydrothermal method and succedent sulfuration. Notably, benefiting from the unique composition, electronic structure, and morphology, the obtained CuCoS/CC exhibits excellent catalytic performance and remarkable durability for OER. When the current density of 10 mA cm$^{-2}$ is driven, the overpotential required is as low as 276 mV, and the Tafel slope achieved is 58 mV decade$^{-1}$, which is lower than the reference $IrO_2$ (304 mV at 10 mA cm$^{-2}$, 62 mV decade$^{-1}$). The experimental results also show that the performance of copper-cobalt composite sulfides for OER is superior to that of $CuS_2$/CC, $CoS_2$/CC, and CuCoO/CC, which suggests that the CuCoS/CC electrode has wide prospects in practical application.

## 2. Results and Discussion

Scheme 1 clearly illustrates the schematic strategy for the synthesis and fabrication of the CuCoS/CC electrode. The original carbon cloths underwent acid soaking, cleaning and annealing, and finally the oxidized carbon cloths were obtained (bare CC). Then, the vertical nanosheets arrays were grown by the one-step hydrothermal method (denoted as CuCo precursor/CC). Subsequently, the as-prepared CuCo precursor/CC was further sulphured at 600 °C in the nitrogen atmosphere, and finally the CuCoS/CC catalyst was obtained. Similarly, the precursor was annealed without adding sulfur in same condition to acquire the CuCo oxides (CuCoO/CC) (all of the details are shown in the Experimental Section).

Figure 1a–b and S1b show the scanning electron microscopy (SEM) images of the CuCo precursor/CC and CuCoO/CC, respectively. A large number of nanosheets grow uniformly and vertically on carbon cloth. Additionally, the surface of nanosheets is smooth without pores, along with neat and non-rough edges. After sulfuration, as shown in Figure 1c–d, the overall structure and morphology of the samples remain intact. However, the surface of the obtained CuCoS/CC becomes rough and porous relative to that of the CuCoO/CC and CuCo precursor/CC, and the thickness of the nanosheets also increases. This effect will lead to the enlargement of specific surface area and introduce some defects, which are conducive to the increase of active sites on the surface and edge of the nanosheets, and enhance the transmission and transfer of electrons and protons [34,35]. Further transmission electron microscopy (TEM) analyses show that the nanosheets have ultrathin structure and transparent edges at some locations (Figure 1e). In high-resolution transmission electron microscopy

(HRTEM) (Figure 1f), the lattice spacing of 0.319 nm can be clearly seen, which matches well with the (111) plane of $CoS_2$. The energy dispersive X-ray spectrum (EDX) illustrates the elemental composition and distribution on the surface of the CuCoS/CC in Figure 1g, showing that the Cu, Co, and S elements are abundant and homogeneously distributed throughout the nanosheets.



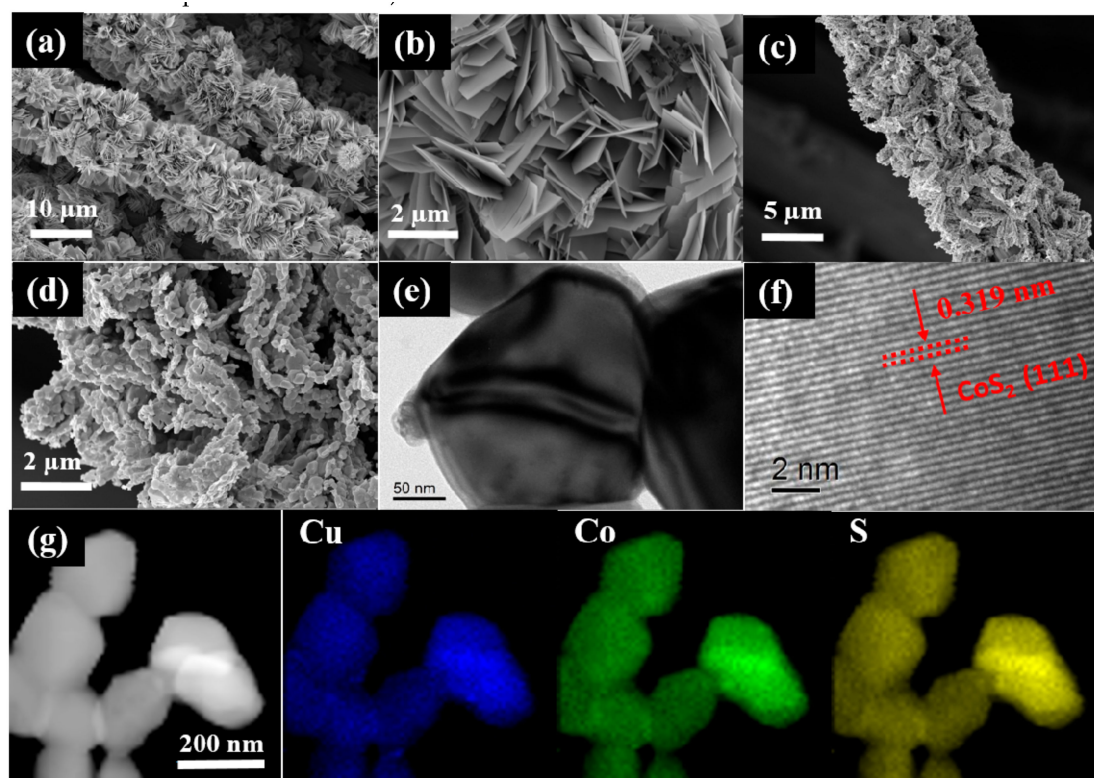**Scheme 1.** Representation of the fabrication process of CuCoS/CC.



**Figure 1.** Scanning electron microscopy (SEM) image of (**a**) and (**b**) CuCo precursor/CC at different magnifications, (**c**) and (**d**) CuCoS/ carbon cloth (CC) at different magnifications. (**e**) Transmission electron microscopy (TEM) and (**f**) high-resolution TEM images of CuCoS/CC. (**g**) TEM image and the corresponding Cu, Co, S element mapping images.

To further understand the intrinsic information of the crystalline phase and components, the X-ray diffraction (XRD) pattern of the CuCoS/CC is collected and shown in Figure 2a. The XRD pattern shows that the CuCoS/CC contains the $CoS_2$ and $CuS_2$ phases, and the diffraction peaks exist between the two standard phases (PDF#89-1492 and PDF#33-0492). This result indicates the formation of the CuCo complex sulfide. From the inductively coupled plasma mass spectrometry (ICP-MS) measurement,

we can find that the percentage of Co and Cu is determined to be 26.78% and 15.34%, respectively (Table S1). Furthermore, the chemical and electronic states of the elements on the surface of the CuCoS/CC are characterized by X-ray photoelectron spectroscopy (XPS). Figure 2b shows the XPS spectra of Cu 2p of CuCoS/CC. The peaks at 934.9 and 954.7 eV are assigned to Cu $2p_{3/2}$ and Cu $2p_{1/2}$, respectively, which is consistent with $Cu^{2+}$. Likewise, two discrete peaks that are situated in 952.3 and 932.5 eV correspond to $Cu^+$. Additionally, satellite peaks can be observed at the binding energy of 943.3 and 963.1 eV (identified as Sat.) [36]. These results suggest that the Cu element of $CuS_2$ phase exists in the valence states of +1 and +2 in the CuCoS/CC. The peaks of Co $2p_{1/2}$ and Co $2p_{3/2}$ appear at 793.9 and 778.7 eV (Figure 2c), respectively, with satellite peaks at 780.9 and 800.5 eV. These above results indicate that $Co^{2+}$ and $Co^{3+}$ coexist in the CuCoS/CC [37]. On the other hand, the peaks at 164 and 162.7 eV are attributed to S $2p_{1/2}$ and S $2p_{3/2}$, respectively (Figure 2d). The peak at 168.9 eV is ascribed to the sulfate species that formed by the interaction of S with $O_2$ adsorbed on the surface [38,39]. Besides, the Raman spectrum of the CuCoS/CC reveals two relatively strong peaks at 1360 and 1590 $cm^{-1}$, which are assigned to irregular defective carbon in D band and graphite carbon in G band, respectively (Figures S2 and S3). The intensity ratio of D peak to G peak is calculated. It is found that the intensity of $I_D/I_G$ of CuCoS/CC (1.08) is slightly higher than that of bare CC (0.94), which implies that sulfuration would lead to some structural distortion, which would in more irregular defects and more active sites [5,21,40]. The hydrophilicity of the CuCoS/CC is also characterized by measuring the interface contact angle. Figure S4 shows the reduced contact angle of the CuCoS/CC (131.29°) as compared to the bare CC (145.16°), which implies that ternary copper-cobalt sulfide nanosheets can contribute to improved surface wettability and increased contact between nanosheets and electrolyte. Based on the analysis of the above characterizations, the successful synthesis of CuCoS/CC is strongly demonstrated.
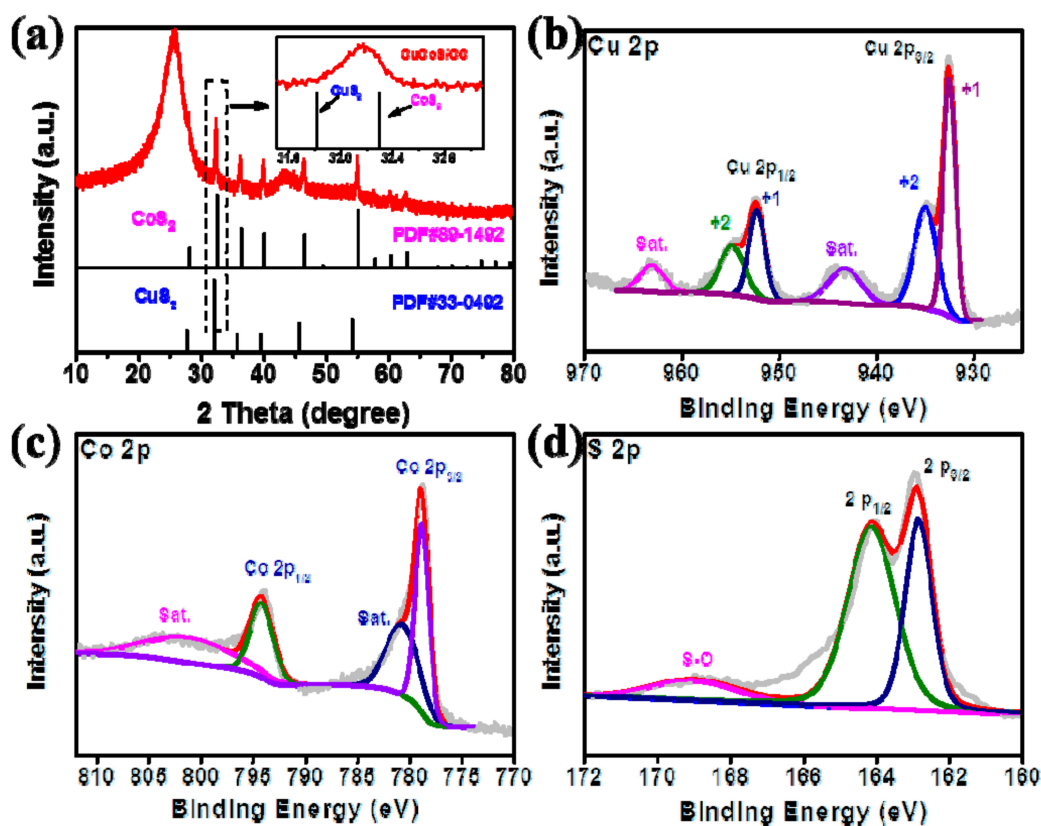


**Figure 2.** (**a**) X-ray diffraction (XRD) pattern of CuCoS/CC. High-resolution X-ray photoelectron spectroscopy (XPS) spectra of (**b**) Cu 2p and (**c**) Co 2p (**d**) S 2p regions of CuCoS/CC.

In order to eValuate the electrocatalytic performance of the synthesized CuCoS/CC for OER, the standard three-electrode system in 1.0 M KOH is applied for characterization. Bare CC, CuCoO/CC, $CoS_2$/CC, $CuS_2$/CC, and $IrO_2$ on CC ($IrO_2$/CC) are also tested in the same condition for comparison. Figure 3a and Figure S5 show the linear sweep voltammetry (LSV) curves of the as-prepared samples at a scan rate of 5 mV s$^{-1}$. To accurately determine the catalytic activity, the overpotential that is required at current density of 10 mA cm$^{-2}$ is used as an index to eValuate the performance, which is related to solar fuel synthesis [41]. Clearly, as shown in Figure 3b, the CuCoS/CC only needs 276 mV overpotential to drive the current density of 10 mA cm$^{-2}$, which is much smaller than that of CuCoO/CC (332 mV), $IrO_2$/CC (304 mV), and bare CC (470 mV). Subsequently, we compare the reported copper-cobalt based catalysts with similar loadings, to better explain the underlying mechanism of improved catalytic performance from different perspectives (Table S2). We adopt the strategy of in-situ growth of CuCoS on carbon cloth, as opposed to materials adhering to the substrate by binders [42]. This is conducive to exposing more active sites and improving electron transport efficiency, which thus promotes the improvement of catalytic activity [43,44]. Besides, when compared with the reported pure $CoS_2$ grown on carbon cloth, the mechanism of our CuCoS/CC's excellent performance is due to the introduction of copper atoms, and the synergistic effect between copper and cobalt is beneficial in improving the catalytic performance [45]. We also contrast the performance of cobalt-based oxides and hydroxides in situ grown on carbon substrates reported, which show poor performance. This further shows that sulfidation can enhance the conductivity and greatly improve the catalytic performance [46,47]. In addition, Tafel slopes are used to examine the kinetic process of electrocatalysis for OER (Figure 3c). CuCoS/CC exhibits a smallest Tafel slope of 58 mV dec$^{-1}$, which is lower than CuCoO/CC (92 mV dec$^{-1}$), $IrO_2$/CC (62 mV dec$^{-1}$), and bare CC (105 mV dec$^{-1}$), suggesting that CuCoS/CC can deprotonate and rearrange OH$^-$ group more quickly than others, which is the rate determining step at lower potential [48–50]. $CoS_2$/CC, $CuS_2$/CC are also tested to confirm the advantages of ternary copper-cobalt sulfides, as shown in Figure S5. As we expected, when the current density is 10 mA cm$^{-2}$, $CoS_2$/CC, and $CuS_2$/CC show overpotentials of 309 mV and 357 mV, severally, which are much higher than CuCoS/CC. The above results prove that the synergistic effect of Cu and Co is beneficial in adjusting the electronic state and increasing the intrinsic activity, thus promoting the improvement of catalytic activity [51,52]. Stability is also a particularly important factor of electrocatalysis. In Figure 3d, after 5000 cycles of cyclic voltammetry, the polarization curve of the CuCoS/CC is almost the same as that of the initial test, with no attenuation, which indicates that the CuCoS/CC has excellent stability.

Next, we calculate the cyclic voltammetric characteristic curve to obtain the electrochemical double-layer capacitance ($C_{dl}$) (Figure 4a–b and Figure S6a), and evaluate the electrochemical surface area (ECSA) to further determine the catalytic performance. Figure 4c indicates that CuCoS/CC has a higher ECSA of 10.92 mF cm$^{-2}$ than CuCoO/CC (7.11 mF cm$^{-2}$) and bare CC (5.12 mF cm$^{-2}$), which thus provides more active sites toward OER dynamic process [53,54]. The electrochemical impedance spectroscopy (EIS) further studies the catalytic activity of OER. As shown in Figure 4d, the Nyquist plots suggest that CuCoS/CC has a smaller semicircle radius, when compared with CuCoO/CC. This indicates that the CuCoS/CC has lower transmission impedance, higher charge transfer rate, and excellent reaction kinetics in OER, where the Randles equivalent circuit is embedded in Figure 4d [55]. As can be seen in Figure S6b, CuCoS/CC reveals a steady rate of hydrogen and oxygen production, which is close to the theoretical value. In the process of water splitting, it also demonstrates that the volume ratio of $H_2$/$O_2$ production matches well with 2:1, and achieves nearly 100% faradaic efficiency, which indicates that very little oxygen is used to produce hydrogen peroxide in the OER process. Accordingly, hydrogen peroxide is seldom generated in the whole electrocatalytic reaction, which illustrates that synthesized CuCoS/CC has higher OER activity and efficiency [56].
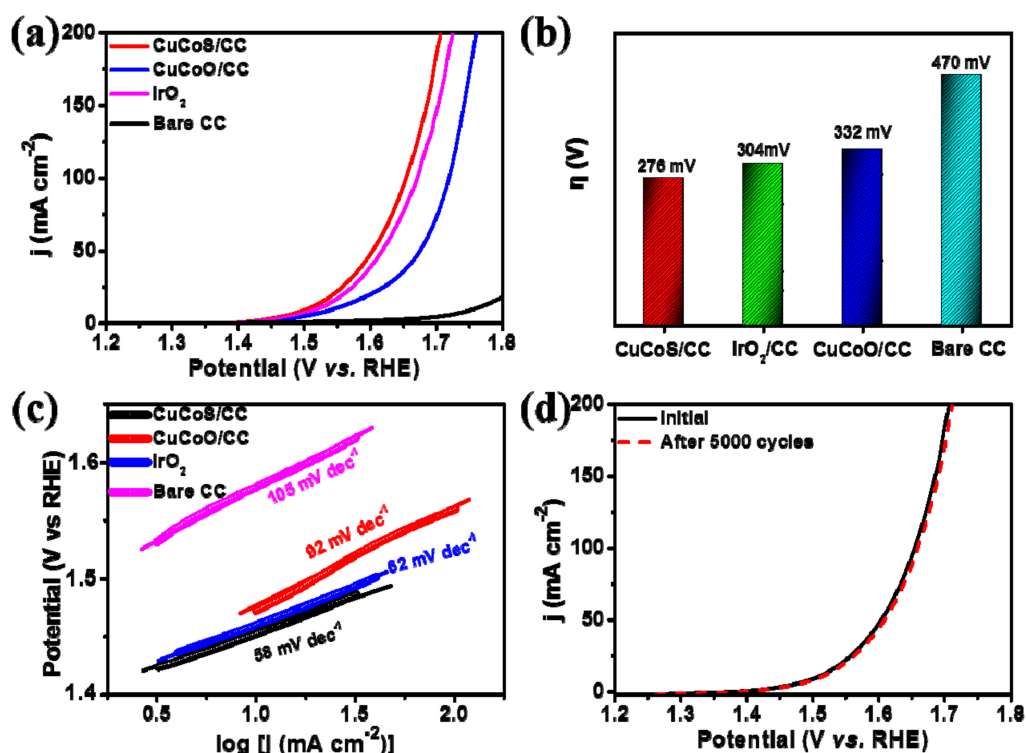
**Figure 3.** (**a**) Polarization curves, (**b**) Comparisons of the potentials required to reach the current density of 10 mA cm$^{-2}$, (**c**) Tafel plots of various catalysts in 1.0 M KOH solution at 5 mV s$^{-1}$ of CuCoS/CC, CuCoO/CC, bare CC and IrO$_2$/CC. (**d**) Linear sweep voltammetry (LSV) curves after 5000 CV cycles for the CuCoS/CC electrode.



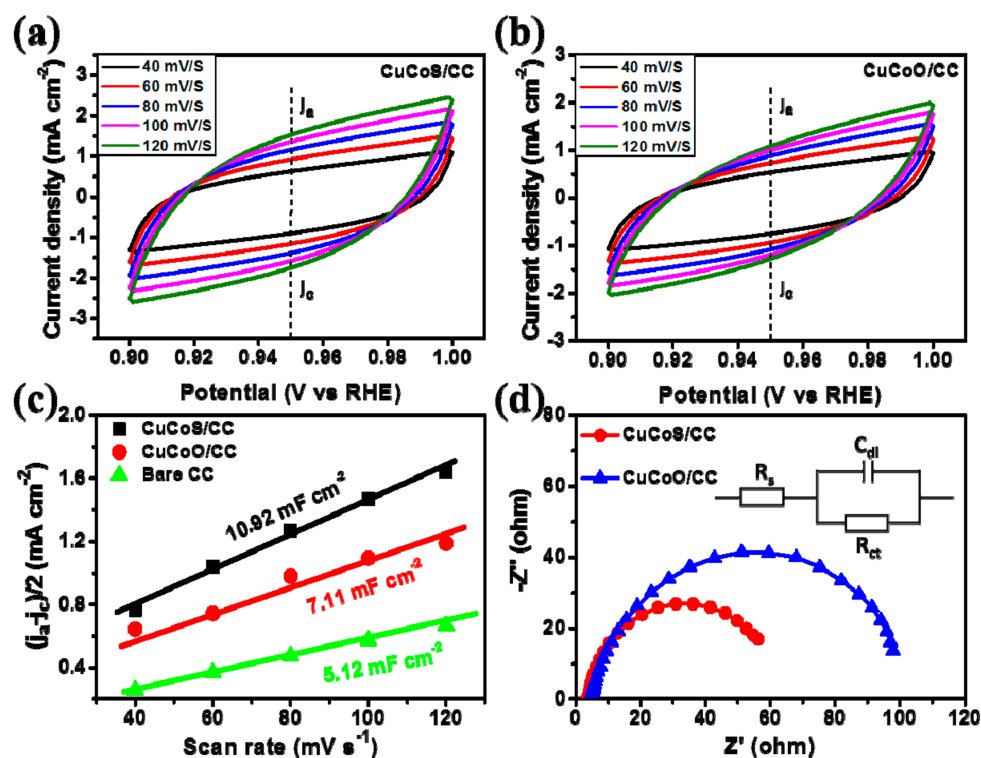**Figure 4.** Cyclic voltammetry of (**a**) CuCoS/CC and (**b**) CuCoO/CC. (**c**) electrochemical surface areas of CuCoS/CC, CuCoO/CC and bare CC. (**d**) Electrochemical impedance spectroscopy plots for CuCoO/CC and CuCoS/CC.

## 3. Materials and Methods

### 3.1. Chemicals and Materials

Commercial carbon clothes (CC WOS 1002) were purchased from PHYCHEMi Co. Ltd., Hongkong. Cobalt nitrate hexahydrate ($Co(NO_3)_2 \cdot 6H_2O$), nafion solution, sulfur powder and Copper nitrate trihydrate ($Cu(NO_3)_2 \cdot 3H_2O$) were purchased from Shanghai Aladdin Bio-Chem Technology Co., Ltd., Shanghai, China, Nitric acid (70% $HNO_3$), urea and sulphuric acid (98% $H_2SO_4$) were purchased from Shanghai Macklin Biochemical Co., Ltd., Shanghai, China.

### 3.2. Syntheses of Oxided Carbon Clothes (Bare CC)

The preparation of oxided carbon clothes is according to previous work [57]. Commercial carbon clothes (WOS 1002) were immersed in a beaker with a mixture of 10 mL of 98% $H_2SO_4$, 10 mL of 70% $HNO_3$, and 10 mL of deionized water, and the area of the infiltration is approximately $1 \times 1\ cm^{-2}$. After that, the beaker was transferred to the drying oven and heated at 70 °C for 24 h. Subsequently, the carbon clothes were washed with a lot of deionized water until its pH was close to 7, followed by dried 60 °C for 24 h. Subsequently, those carbon clothes were heated in a muffle furnace to 500 °C at a heating rate of 10 °C min$^{-1}$ for 2 h. Next, we cut 1 cm × 0.5 cm carbon cloth for further use.

### 3.3. Syntheses of CuCoS/CC

In a typical synthetic process, 60.4 mg $Cu(NO_3)_2 \cdot 3H_2O$, 146 mg $Co(NO_3)_2 \cdot 6H_2O$, and 180 mg urea were dissolved into 20 mL deionized water and then stirring to form a uniform solution. Among them, urea exhibits good chelating ability, enhances the solubility of solvent, and contributes to the formation of CuCo based nanosheets structure, along with the production of $NH_3$ in the hydrothermal reaction, adjusting the pH value of the solvent [58]. Subsequently, the mixture and oxided carbon clothes were transferred to a Teflon-lined stainless steel autoclave (50 mL), which was heated at 120 °C for 5 h. After the autoclave was cooled to room temperature, the samples were washed with deionized water and then dried at 60 °C in vacuum. Finally, the samples that were covered with S powder (2 g) were placed in a corundum boat and calcinated in a tube furnace to 600 °C at a rate of 5 °C min$^{-1}$ for 2 h under the flowing $N_2$ atmosphere. The CuCoO/CC was prepared in the same manner, except that no S powder added. The catalysts loading on the CC were calculated about 1 mg cm$^{-2}$. For synthesizing $CuS_2$/CC and $CoS_2$/CC, the method is same above-mentioned process, just without added $Co(NO_3)_2 \cdot 3H_2O$ and $Cu(NO_3)_2 \cdot 6H_2O$, respectively.

### 3.4. Characterization

The phase purity of the samples was identified from its X-ray diffraction pattern that was obtained on an X-ray diffractometer (Rigaku Smartlab) using Cu K$\alpha$ radiation (40 kV, 40 mA). Field emission scanning electron microscopy (SEM, Hitachi SU8010) and transmission electron microscopy (TEM, FEI Tecnai G2 F20) equipped with an energy-dispersive spectrometer (EDS) characterized the morphologies and ingredient of the as-synthesized samples. Raman spectra were recorded by confocal Raman microscope (LabRAM HR eVolution) with 532 nm laser excitation. X-ray photoelectron spectroscopy (XPS) results were performed using Thermo ESCALAB 250XI. The contact angle analysis was recorded by an optical contact angle measuring instrument (JY-82B). The dioxygen yield was measured by gas chromatography (GC) analysis (FULI GC 9790II) purchased from Zhejiang FULI Analytical Instrument Co., Ltd., Zhengjiang, China. The moles of metal in CuCoS/CC were determined based on the inductively coupled plasma-optical emmision spectrometry (ICP–OES) results (Table S1, Supporting Information).

*3.5. Electrochemical Measurements*

The electrochemical measurements of OER were recorded by a three-electrode system with an electrochemical workstation (CHI 660, Shanghai Chenhua, Shanghai, China). The CuCoS/CC was used as a directly working electrode, and the Pt sheet was used as a counter electrode and the saturated Hg/HgO served as the reference electrode, respectively. An ion exchange membrane was applied to separate the working from the counter electrode. The geometric area of the carbon cloth normalized all of the measured current densities (1 cm × 0.5 cm). As for the $IrO_2$/CC, 5 mg of catalysts were dispersed in 1 mL of ethanol and 20 μL of nafion solution by sonication, forming homogeneous ink, and then dropped onto CC with the loading about 1 mg/cm$^{-2}$. Linear sweep voltammetry for OER and cyclic voltammograms were conducted in 1.0 M KOH. The linear sweep voltammetry was iR-corrected. Electrochemical impedance spectra were measured from 10 kHz to 100 mHz with an amplitude of 5 mV. The cyclic voltammograms curves were measured at the potential range from 0.90 to 1.00 V versus RHE at scan rate of 40, 60, 80, 100, 120 mV s$^{-1}$. In the voltage range of 0–0.5 V with the scan rate of 100 mV/s, the stability test was performed after 5000 cycles of CV test. The potential readings were reported with respect to RHE according to the Nernst equation: $E_{RHE} = E_{Hg/HgO} + 0.059 \times pH + 0.098$. The following formula are usually used to calculate ESCA: $S_{ECSA} = (C_{dl} \times S_{GEO})/SC$. SC stands for specific capacitance, generally ranging from 20 to 60 μF cm$^{-2}_{ECSA}$, and SGEO represents the geometric area of the electrode. $C_{dl}$ can be obtained from cyclic voltammograms (CVs) at different scan rates [59].

## 4. Conclusions

In summary, we have demonstrated the successful design and synthesis of CuCoS/CC by a hydrothermal method accompanied by the direct sulfidation of CuCo-based precursors. The CuCoS/CC reveals prominent electrocatalytic activity with a lower overpotential of only 276 mV at a current density of 10 mA cm$^{-2}$ and Tafel slope of 58 mV dec$^{-1}$ in 1.0 M KOH, which is superior to commercial $IrO_2$. In addition, the mechanism of significant enhancement of catalytic performance of CuCoS/CC has also been explored, to a certain extent. The synergistic effect of Cu and Co atoms is propitious to optimize the electronic structure and enhance the intrinsic activity of materials. Additionally, sulfidation enriches the active sites of the CuCoS/CC and it promotes the electrocatalytic reaction kinetics for OER. When combined with the advantages of excellent properties of CuCoS/CC, simple preparation and synthesis method, and abundant sources on the earth, it has the enormous potential to replace noble metal catalysts and provide promising ideas for practical application.

**Author Contributions:** H.L. (Heng Luo) and H.L. (Hang Lei) contributed equally to this work. Conceptualization, H.L. (Heng Luo) and H.L. (Hang Lei); methodology, H.L. (Heng Luo) and H.L. (Hang Lei); synthesis and characterizations, H.L. (Hang Lei), Y.Y., Y.L. and Y.Q.; manuscript writing, H.L. (Heng Luo); supervision, Z.Z., Z.W.; project administration, Z.W.; funding acquisition, Z.W. All authors commented on the manuscript and agreed on the final version.

**Conflicts of Interest:** The authors declare no conflict of interest.

## References

1. Seh, Z.W.; Kibsgaard, J.; Dickens, C.F.; Chorkendorff, I.; Nørskov, J.K.; Jaramillo, T.F. Combining theory and experiment in electrocatalysis: Insights into materials design. *Science* **2017**, *355*, eaad4998. [CrossRef]

2. Jiao, Y.; Zheng, Y.; Jaroniec, M.; Qiao, S.Z. Design of electrocatalysts for oxygen-and hydrogen-involving energy conversion reactions. *Chem. Soc. Rev.* **2015**, *44*, 2060–2086. [CrossRef]

3. Tian, T.; Gao, H.; Zhou, X.; Zheng, L.; Wu, J.; Li, K.; Ding, Y. Study of the Active Sites in Porous Nickel Oxide Nanosheets by Manganese Modulation for Enhanced Oxygen eVolution Catalysis. *ACS Energy Lett.* **2018**, *3*, 2150–2158. [CrossRef]

4. Cho, S.-H.; Yoon, K.R.; Shin, K.; Jung, J.-W.; Kim, C.; Cheong, J.Y.; Youn, D.-Y.; Song, S.W.; Henkelman, G.; Kim, I.-D. Synergistic Coupling of Metallic Cobalt Nitride Nanofibers and IrOx Nanoparticle Catalysts for Stable Oxygen eVolution. *Chem. Mater.* **2018**, *30*, 5941–5950. [CrossRef]

5. Zheng, J.; Chen, X.; Zhong, X.; Li, S.; Liu, T.; Zhuang, G.; Li, X.; Deng, S.; Mei, D.; Wang, J.G. Hierarchical porous NC@CuCo nitride nanosheet networks: Highly efficient bifunctional electrocatalyst for overall water splitting and selective electrooxidation of benzyl alcohol. *Adv. Funct. Mater.* **2017**, *27*, 1704169. [CrossRef]

6. Pirkarami, A.; Rasouli, S.; Ghasemi, E. 3-D CdS@ NiCo layered double hydroxide core-shell photoelectrocatalyst used for efficient overall water splitting. *Appl. Catal. B: Environ.* **2019**, *241*, 28–40. [CrossRef]

7. Wang, Y.; Yan, D.; El Hankari, S.; Zou, Y.; Wang, S. Recent progress on layered double hydroxides and their derivatives for electrocatalytic water splitting. *Adv. Sci.* **2018**, *5*, 1800064. [CrossRef] [PubMed]

8. Ding, Q.; Song, B.; Xu, P.; Jin, S. Efficient electrocatalytic and photoelectrochemical hydrogen generation using $MoS_2$ and related compounds. *Chem* **2016**, *1*, 699–726. [CrossRef]

9. Shao, W.; Xia, Y.; Luo, X.; Bai, L.; Zhang, J.; Sun, G.; Xie, C.; Zhang, X.; Yan, W.; Xie, Y. Structurally distorted wolframite-type $CoxFe_{1-x}WO_4$ solid solution for enhanced oxygen eVolution reaction. *Nano Energy* **2018**, *50*, 717–722. [CrossRef]

10. Sanchez, J.; Ramos-Garcés, M.V.; Narkeviciute, I.; Colón, J.L.; Jaramillo, T.F. Transition Metal-Modified Zirconium Phosphate Electrocatalysts for the Oxygen eVolution Reaction. *Catalysts* **2017**, *7*, 132. [CrossRef]

11. Chen, P.; Zhou, T.; Wang, S.; Zhang, N.; Tong, Y.; Ju, H.; Chu, W.; Wu, C.; Xie, Y. Dynamic Migration of Surface Fluorine Anions on Cobalt-Based Materials to Achieve Enhanced Oxygen eVolution Catalysis. *Angew. Chem. Int. Ed.* **2018**, *57*, 15471–15475. [CrossRef]

12. Kim, B.K.; Kim, S.-K.; Cho, S.K.; Kim, J.J. Enhanced catalytic activity of electrodeposited Ni-Cu-P toward oxygen eVolution reaction. *Appl. Catal. B: Environ.* **2018**, *237*, 409–415. [CrossRef]

13. Chauhan, M.; Reddy, K.P.; Gopinath, C.S.; Deka, S. Copper cobalt sulfide nanosheets realizing a promising electrocatalytic oxygen eVolution reaction. *ACS Catal.* **2017**, *7*, 5871–5879. [CrossRef]

14. Xu, H.; Cao, J.; Shan, C.; Wang, B.; Xi, P.; Liu, W.; Tang, Y. MOF-Derived Hollow CoS Decorated with CeOx Nanoparticles for Boosting Oxygen eVolution Reaction Electrocatalysis. *Angew. Chem.* **2018**, *130*, 8790–8794. [CrossRef]

15. Paulraj, A.; Kiros, Y.; Göthelid, M.; Johansson, M. Nifeox as a bifunctional electrocatalyst for oxygen reduction (OR) and eVolution (OE) reaction in alkaline media. *Catalysts* **2018**, *8*, 328. [CrossRef]

16. Guo, C.; Sun, X.; Kuang, X.; Gao, L.; Zhao, M.; Qu, L.; Zhang, Y.; Wu, D.; Ren, X.; Wei, Q. Amorphous Co-doped MoO x nanospheres with a core–shell structure toward an effective oxygen eVolution reaction. *J. Mater. Chem. A* **2019**, *7*, 1005–1012. [CrossRef]

17. Ohno, H.; Nohara, S.; Kakinuma, K.; Uchida, M.; Uchida, H. Effect of Electronic Conductivities of Iridium Oxide/Doped $SnO_2$ Oxygen-Evolving Catalysts on the Polarization Properties in Proton Exchange Membrane Water Electrolysis. *Catalysts* **2019**, *9*, 74. [CrossRef]

18. Ryu, S.; Hoffmann, M. Mixed-metal semiconductor anodes for electrochemical water splitting and reactive chlorine species generation: Implications for electrochemical wastewater treatment. *Catalysts* **2016**, *6*, 59. [CrossRef]

19. Han, H.; Kim, K.M.; Choi, H.; Ali, G.; Chung, K.Y.; Hong, Y.-R.; Choi, J.; Kwon, J.; Lee, S.W.; Lee, J.W. Parallelized reaction pathway and stronger internal band bending by partial oxidation of metal sulfide–graphene composites: Important factors of synergistic oxygen eVolution reaction enhancement. *ACS Catal.* **2018**, *8*, 4091–4102. [CrossRef]

20. Yu, L.; Yang, J.F.; Lou, X.W. Formation of $CoS_2$ nanobubble hollow prisms for highly reversible lithium storage. *Angew. Chem. Int. Ed.* **2016**, *55*, 13422–13426. [CrossRef]

21. Liu, W.; Zhang, J.; Bai, Z.; Jiang, G.; Li, M.; Feng, K.; Yang, L.; Ding, Y.; Yu, T.; Chen, Z. Controllable Urchin-Like NiCo$_2$S$_4$ Microsphere Synergized with Sulfur-Doped Graphene as Bifunctional Catalyst for Superior Rechargeable Zn–Air Battery. *Adv. Funct. Mater.* **2018**, *28*, 1706675. [CrossRef]

22. Ge, Y.; Wu, J.; Xu, X.; Ye, M.; Shen, J. Facile synthesis of CoNi$_2$S$_4$ and CuCo$_2$S$_4$ with different morphologies as prominent catalysts for hydrogen eVolution reaction. *Int. J. Hydrogen Energy* **2016**, *41*, 19847–19854. [CrossRef]

23. Ma, X.; Zhang, W.; Deng, Y.; Zhong, C.; Hu, W.; Han, X. Phase and composition controlled synthesis of cobalt sulfide hollow nanospheres for electrocatalytic water splitting. *Nanoscale* **2018**, *10*, 4816–4824. [CrossRef]

24. Du, X.; Zhang, X.; Yang, Z.; Gong, Y. Water Oxidation Catalysis Beginning with CuCo$_2$S$_4$: Investigation of the True Electrochemically Driven Catalyst. *Chem. Asian J.* **2018**, *13*, 266–270. [CrossRef]

25. Zequine, C.; Bhoyate, S.; Wang, F.; Li, X.; Siam, K.; Kahol, P.; Gupta, R.K. Effect of solvent for tailoring the nanomorphology of multinary CuCo$_2$S$_4$ for overall water splitting and energy storage. *J. Alloys Compd.* **2019**, *784*, 1–7. [CrossRef]

26. Coughlan, C.; Ibanez, M.; Dobrozhan, O.; Singh, A.; Cabot, A.; Ryan, K.M. Compound copper chalcogenide nanocrystals. *Chem. Rev.* **2017**, *117*, 5865–6109. [CrossRef]

27. Zhang, J.; Bai, X.; Wang, T.; Xiao, W.; Xi, P.; Wang, J.; Gao, D.; Wang, J. Bimetallic Nickel Cobalt Sulfide as Efficient Electrocatalyst for Zn–Air Battery and Water Splitting. *Nano-Micro Lett.* **2019**, *11*, 2. [CrossRef]

28. Zhang, J.; Xiao, B.; Liu, X.; Liu, P.; Xi, P.; Xiao, W.; Ding, J.; Gao, D.; Xue, D. Copper dopants improved the hydrogen eVolution activity of earth-abundant cobalt pyrite catalysts by activating the electrocatalytically inert sulfur sites. *J. Mater. Chem. A* **2017**, *5*, 17601–17608. [CrossRef]

29. Irshad, A.; Munichandraiah, N. Electrodeposited nickel–cobalt–sulfide catalyst for the hydrogen eVolution reaction. *ACS Appl. Mater. Interfaces* **2017**, *9*, 19746–19755. [CrossRef] [PubMed]

30. Koh, S.; Strasser, P. Electrocatalysis on bimetallic surfaces: modifying catalytic reactivity for oxygen reduction by voltammetric surface dealloying. *J. Am. Chem. Soc.* **2007**, *129*, 12624–12625. [CrossRef] [PubMed]

31. Guo, S.; Chen, W.; Li, M.; Wang, J.; Liu, F.; Cheng, J. Effect of reaction temperature on the amorphous-crystalline transition of copper cobalt sulfide for supercapacitors. *Electrochim. Acta* **2018**, *271*, 498–506. [CrossRef]

32. Guo, M.; Balamurugan, J.; Thanh, T.D.; Kim, N.H.; Lee, J.H. Facile fabrication of Co$_2$CuS$_4$ nanoparticle anchored N-doped graphene for high-performance asymmetric supercapacitors. *J. Mater. Chem. A* **2016**, *4*, 17560–17571. [CrossRef]

33. Liu, S.; Yin, Y.; Hui, K.S.; Hui, K.N.; Lee, S.C.; Jun, S.C. High-Performance Flexible Quasi-Solid-State Supercapacitors Realized by Molybdenum Dioxide@ Nitrogen-Doped Carbon and Copper Cobalt Sulfide Tubular Nanostructures. *Adv. Sci.* **2018**, *5*, 1800733. [CrossRef] [PubMed]

34. Yang, J.; Wang, C.; Ju, H.; Sun, Y.; Xing, S.; Zhu, J.; Yang, Q. Integrated quasiplane heteronanostructures of MoSe$_2$/Bi$_2$Se$_3$ hexagonal nanosheets: synergetic electrocatalytic water splitting and enhanced supercapacitor performance. *Adv. Funct. Mater.* **2017**, *27*, 1703864. [CrossRef]

35. Zhang, C.; Bhoyate, S.; Zhao, C.; Kahol, P.K.; Kostoglou, N.; Mitterer, C.; Hinder, S.J.; Baker, M.A.; Constantinides, G.; Polychronopoulou, K. Electrodeposited Nanostructured CoFe$_2$O$_4$ for Overall Water Splitting and Supercapacitor Applications. *Catalysts* **2019**, *9*, 176. [CrossRef]

36. Yu, J.; Zhang, J.; Liu, S. Ion-exchange synthesis and enhanced visible-light photoactivity of CuS/ZnS nanocomposite hollow spheres. *J. Phys. Chem. C* **2010**, *114*, 13642–13649. [CrossRef]

37. Li, B.; Yuan, F.; He, G.; Han, X.; Wang, X.; Qin, J.; Guo, Z.X.; Lu, X.; Wang, Q.; Parkin, I.P. Ultrasmall CuCo$_2$S$_4$ Nanocrystals: All-in-One Theragnosis Nanoplatform with Magnetic Resonance/Near-Infrared Imaging for Efficiently Photothermal Therapy of Tumors. *Adv. Funct. Mater.* **2017**, *27*, 1606218. [CrossRef]

38. Hou, Z.; Shu, C.; Long, J. Honeycomb-like Ni$_3$S$_2$ supported on Ni foam as high performance free-standing cathode for lithium oxygen batteries. *Electrochim. Acta* **2018**, *290*, 657–665. [CrossRef]

39. Czioska, S.; Wang, J.; Teng, X.; Chen, Z. Hierarchically structured CuCo$_2$S$_4$ nanowire arrays as efficient bifunctional electrocatalyst for overall water splitting. *ACS Sustain. Chem. Eng.* **2018**, *6*, 11877–11883. [CrossRef]

40. Sivanantham, A.; Ganesan, P.; Shanmugam, S. A synergistic effect of Co and CeO$_2$ in nitrogen-doped carbon nanostructure for the enhanced oxygen electrode activity and stability. *Appl. Catal. B Environ.* **2018**, *237*, 1148–1159. [CrossRef]

41. Yang, J.; Zhu, G.; Liu, Y.; Xia, J.; Ji, Z.; Shen, X.; Wu, S. $Fe_3O_4$-Decorated $Co_9S_8$ Nanoparticles In Situ Grown on Reduced Graphene Oxide: A New and Efficient Electrocatalyst for Oxygen eVolution Reaction. *Adv. Funct. Mater.* **2016**, *26*, 4712–4721. [CrossRef]

42. Meng, F.; Zhong, H.; Bao, D.; Yan, J.; Zhang, X. In situ coupling of strung $Co_4N$ and intertwined N–C fibers toward free-standing bifunctional cathode for robust, efficient, and flexible Zn–air batteries. *J. Am. Chem. Soc.* **2016**, *138*, 10226–10231. [CrossRef]

43. Lin, R.; Lei, H.; Ruan, D.; Jiang, K.; Yu, X.; Wang, Z.; Mai, W.; Yan, H. Solar-powered overall water splitting system combing metal-organic frameworks derived bimetallic nanohybrids based electrocatalysts and one organic solar cell. *Nano Energy* **2019**, *56*, 82–91. [CrossRef]

44. Li, Q.; Wang, X.; Tang, K.; Wang, M.; Wang, C.; Yan, C. Electronic modulation of electrocatalytically active center of $Cu_7S_4$ nanodisks by cobalt-doping for highly efficient oxygen eVolution reaction. *ACS Nano* **2017**, *11*, 12230–12239. [CrossRef]

45. Deng, Y.H.; Ye, C.; Tao, B.X.; Chen, G.; Zhang, Q.; Luo, H.Q.; Li, N.B. One-step chemical transformation synthesis of $CoS_2$ nanosheets on carbon cloth as a 3D flexible electrode for water oxidation. *J. Power Sources* **2018**, *397*, 44–51. [CrossRef]

46. Kou, Y.; Liu, J.; Li, Y.; Qu, S.; Ma, C.; Song, Z.; Han, X.; Deng, Y.; Hu, W.; Zhong, C. Electrochemical Oxidation of Chlorine-Doped $Co(OH)_2$ Nanosheet Arrays on Carbon Cloth as a Bifunctional Oxygen Electrode. *ACS Appl. Mater. Interfaces* **2017**, *10*, 796–805. [CrossRef]

47. Kargar, A.; Yavuz, S.; Kim, T.K.; Liu, C.-H.; Kuru, C.; Rustomji, C.S.; Jin, S.; Bandaru, P.R. Solution-processed $CoFe_2O_4$ nanoparticles on 3D carbon fiber papers for durable oxygen eVolution reaction. *ACS Appl. Mater. Interfaces* **2015**, *7*, 17851–17856. [CrossRef]

48. Fang, Y.-H.; Liu, Z.-P. Mechanism and tafel lines of electro-oxidation of water to oxygen on $RuO_2$ (110). *J. Am. Chem. Soc.* **2010**, *132*, 18214–18222. [CrossRef]

49. Wang, H.Y.; Hsu, Y.Y.; Chen, R.; Chan, T.S.; Chen, H.M.; Liu, B. $Ni^{3+}$-Induced Formation of Active NiOOH on the Spinel Ni–Co Oxide Surface for Efficient Oxygen eVolution Reaction. *Adv. Energy Mater.* **2015**, *5*, 1500091. [CrossRef]

50. She, S.; Zhu, Y.; Chen, Y.; Lu, Q.; Zhou, W.; Shao, Z. Realizing Ultrafast Oxygen eVolution by Introducing Proton Acceptor into Perovskites. *Adv. Energy Mater.* **2019**, 1900429. [CrossRef]

51. Jin, H.; Mao, S.; Zhan, G.; Xu, F.; Bao, X.; Wang, Y. Fe incorporated α-$Co(OH)_2$ nanosheets with remarkably improved activity towards the oxygen eVolution reaction. *J. Mater. Chem. A* **2017**, *5*, 1078–1084. [CrossRef]

52. Xiong, X.; You, C.; Liu, Z.; Asiri, A.M.; Sun, X. Co-doped CuO nanoarray: an efficient oxygen eVolution reaction electrocatalyst with enhanced activity. *ACS Sustainable Chem. Eng.* **2018**, *6*, 2883–2887. [CrossRef]

53. Fan, K.; Chen, H.; Ji, Y.; Huang, H.; Claesson, P.M.; Daniel, Q.; Philippe, B.; Rensmo, H.; Li, F.; Luo, Y. Nickel–vanadium monolayer double hydroxide for efficient electrochemical water oxidation. *Nat. Commun.* **2016**, *7*, 11981. [CrossRef]

54. Vij, V.; Sultan, S.; Harzandi, A.M.; Meena, A.; Tiwari, J.N.; Lee, W.-G.; Yoon, T.; Kim, K.S. Nickel-based electrocatalysts for energy-related applications: oxygen reduction, oxygen eVolution, and hydrogen eVolution reactions. *ACS Catal.* **2017**, *7*, 7196–7225. [CrossRef]

55. Zou, X.; Goswami, A.; Asefa, T. Efficient noble metal-free (electro) catalysis of water and alcohol oxidations by zinc–cobalt layered double hydroxide. *J. Am. Chem. Soc.* **2013**, *135*, 17242–17245. [CrossRef] [PubMed]

56. Campos-Martin, J.M.; Blanco-Brieva, G.; Fierro, J.L. Hydrogen peroxide synthesis: an outlook beyond the anthraquinone process. *Angew. Chem. Int. Ed.* **2006**, *45*, 6962–6984. [CrossRef] [PubMed]

57. Kordek, K.; Jiang, L.; Fan, K.; Zhu, Z.; Xu, L.; Al-Mamun, M.; Dou, Y.; Chen, S.; Liu, P.; Yin, H. Two-Step Activated Carbon Cloth with Oxygen-Rich Functional Groups as a High-Performance Additive-Free Air Electrode for Flexible Zinc–Air Batteries. *Adv. Energy Mater.* **2018**, 1802936. [CrossRef]

58. Bennion, B.J.; Daggett, V. The molecular basis for the chemical denaturation of proteins by urea. *Proc. Natl. Acad. Sci. USA* **2003**, *100*, 5142–5147. [CrossRef]

59. Yang, Y.; Zhang, W.; Xiao, Y.; Shi, Z.; Cao, X.; Tang, Y.; Gao, Q. $CoNiSe_2$ heteronanorods decorated with layered-double-hydroxides for efficient hydrogen eVolution. *Appl. Catal. B Environ.* **2019**, *242*, 132–139. [CrossRef]